Quantum heat engine based on quantum interferometry: The SU(1,1) Otto cycle

Alessandro Ferreri [1,2,*] Hui Wang (王惠) [2,3] Franco Nori (野理) [2,4,5]
Frank K. Wilhelm [1,6] and David Edward Bruschi [1,6,†]

[1]*Institute for Quantum Computing Analytics (PGI-12), Forschungszentrum Jülich, 52425 Jülich, Germany*
[2]*Theoretical Quantum Physics Laboratory, RIKEN, Wako-shi, Saitama 351-0198, Japan*
[3]*Institute for Quantum Science and Engineering, Texas A&M University, College Station, Texas 77843, USA*
[4]*Center for Quantum Computing, RIKEN, Wako-shi, Saitama 351-0198, Japan*
[5]*Physics Department, The University of Michigan, Ann Arbor, Michigan 48109-1040, USA*
[6]*Theoretical Physics, Universität des Saarlandes, 66123 Saarbrücken, Germany*

We present a quantum heat engine based on a quantum Otto cycle whose working substance reproduces the same outcomes as an SU(1, 1) interference process at the end of each adiabatic transformation. This device takes advantage of the extraordinary quantum metrological features of the SU(1, 1) interferometer to better discriminate the sources of uncertainty of relevant observables during each adiabatic stroke of the cycle. In particular, the SU(1, 1) adiabatic transformations enable high-precision estimations of the energy extracted from the adiabatic stroke, despite the presence of thermal fluctuations. Applications to circuit QED platforms are also discussed.

I. INTRODUCTION

The advent of quantum thermodynamics marks the beginning of a modern way of conceiving the laws of thermodynamics [1–7]. Whereas classical thermodynamics relies its predictions on the statistical behavior of large systems characterized by an uncountable number of components (e.g., the molecules of a gas confined in a piston), quantum thermodynamics studies concepts such as heat transport, entropy production, and work extraction at the quantum scale. One of the main goals within this framework is to miniaturize heat engines by utilizing standard quantum systems, such as qubits or quantum harmonic oscillators, as working substance [8–20].

A quantum heat engine (QHE) is a quantum apparatus that performs a thermodynamic cycle from which one wishes to extract net work [21–32]. In quantum thermodynamics it is possible to define thermodynamic cycles, in complete analogy to the classical counterpart, that depend on the specific transformations performed by the system [8,9]. An example of a thermodynamic cycle largely considered in literature is the quantum Otto cycle [8,33,34], which consists of two adiabatic transformations and two isochoric transformations. At the quantum level, the isochoric transformation is equivalent to the thermalization of the working substance with the hot or cold bath, while the eigenenergies of the system remain constant. On the other hand, during each adiabatic transformation the quantum system is isolated, and its eigenenergies change by means of an external drive.

The working substance releases net work during the adiabatic expansion. Nevertheless, the generation of work does not necessarily imply the release of power. This is the case when the adiabatic transformation occurs quasistatically, for example. For technological purposes it is generally of greater interest to consider more practical scenarios, wherein transformations occur in finite time [35–38], such that one can extract power from the working substance [39–43]. In this case, it may happen that the release of power is affected by inner friction, which means that the system is still not exchanging heat with the environment (classical adiabatic condition), but the population varies during the transformation [44,45].

In this work we propose a quantum heat engine subject to inner friction that performs an Otto cycle whose adiabatic transformations mimic the outcome of the SU(1, 1) interferometer. The SU(1, 1) interferometer is a nonlinear interferometer that is constituted by active optical elements [46–48]. In particular, it can be engineered from the standard Mach-Zehnder interferometer (MZI) by replacing the two beam splitters with two squeezers [49]. The nonlinearity of the interferometer stems from the nonlinear susceptibility of the media typically used as a squeezing resource [50,51].

In quantum metrology, there are several advantages of using SU(1, 1) interferometers with respect to other platforms, such as the Mach-Zehnder interferometer. For example, it has

---

*Contact author: a.ferreri@fz-juelich.de

†Contact author: david.edward.bruschi@posteo.net; d.e.bruschi@fz-juelich.de

been shown that such devices are highly immune to external losses [52]. Moreover, they can overcome the classical shot noise limit and reach the so-called Heisenberg limit even when seeded with the vacuum state [46]. For these reasons, this class of interferometers has been thoroughly studied in the past, for example, by analyzing the role of different input states [53–55], as well as specializing to both spectral and spatial multimode scenarios [50,51,56,57].

The Otto cycle proposed in this work is based on two interacting quantum harmonic oscillators, whose time evolution is modeled in terms of elements of the $\mathfrak{su}(1,1)$ Lie algebra. In particular, our device exploits the equivalence between the output values of the observables after each adiabatic transformations and the outcomes at the end of an $SU(1,1)$ interference scheme to improve our knowledge about such observables beyond the shot-noise limit. Indeed, taking for granted that all observables of interest are affected by quantum fluctuations, we may ask if the uncertainty of our outcomes stems from the instability of the protocols controlling the adiabatic transformations, or from the quantum or thermal fluctuation of the observables themselves. To answer this question, we encode the information about our protocols into the phase of an equivalent $SU(1,1)$ interferometer and study the dependence of the phase sensitivity of the heat engine with respect to both the number of excitations and the average energy at the end of the adiabatic transformations, benchmarking it with the shot-noise limit.

The phase sensitivity is a tool largely used in quantum metrology for estimating the minimal modulation of the phase needed to overcome the quantum (or in this case thermal) fluctuation of observables. In this work, the phase sensitivity is utilized as a tool to optimize the protocols such that, at the end of the adiabatic strokes, we can safely distinguish possible errors due to the instability of our protocols from the perturbation generated by the thermal fluctuations. We show that by increasing the amount of squeezing, while at the same time properly manipulating the internal phase, our device can work simultaneously as a quantum thermal machine performing the Otto cycle with a net work output, as well as an $SU(1,1)$ interferometer working beyond the shot-noise limit.

The paper is structured as follows: in Sec. II we review the mathematical tools to describe the two-mode $SU(1,1)$ interferometer as well as the concept of phase sensitivity. In Sec. III we introduce our model of $SU(1,1)$ heat engine, with focus on the analogy between the outputs of the adiabatic transformations and the outputs of an $SU(1,1)$ interference scenario. In Sec. IV we examine the performance of the QHE by analyzing both the efficiency of the cycle and the phase sensitivity at the end of the adiabatic expansion. We also discuss a superconducting platform where our model can be implemented. We report our conclusions in Sec. V.

II. THEORETICAL BACKGROUND

In this section we introduce the formalism to study the system of interest. In particular, we first present the algebraic tools to describe the $SU(1,1)$ interferometer. Afterwards, we provide a short review of the concept of phase sensitivity and noise limits in quantum metrology.
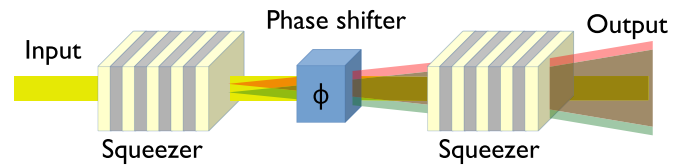

FIG. 1. Design of the SU(1,1) interferometer. The input channel is seeded with a classical source (pump laser), which interacts with two squeezing sources (nonlinear optical media) in order to generate photon pairs. In the degenerate scheme, the created photons may be distinguished by their polarization. The two squeezers are separated by a phase shifter, which controls the relative phase between the laser and the photon pairs.

A. The SU(1, 1) interferometer

The $SU(1,1)$ interferometer is schematically depicted in Fig. 1 and consists of a sequence of squeezing and phase operations: squeezing $\rightarrow$ phase shift $\rightarrow$ antisqueezing [46]. The unitary transformation encoding the interference process takes the form

$$\hat{U}_{su}(\zeta, \phi) = e^{-i\zeta\hat{K}_x} e^{-i\phi\hat{K}_z} e^{i\zeta\hat{K}_x}, \tag{1}$$

where ζ and ϕ identify the squeezing and the phase parameters, respectively.

The operators K_i with $i = $ x, y, z fulfill the following commutation relations,

$$[\hat{K}_j, \hat{K}_k] = i f_{jk\ell} K_\ell, \tag{2}$$

which define the $\mathfrak{su}(1,1)$ Lie algebra with structure constants f_{abc} that read $f_{xyz} = -1$, $f_{yzx} = 1$, $f_{zxy} = 1$, while the only other nonvanishing expressions can be obtained by permutations of the indices in the standard fashion. The Lie algebra is fully defined by the commutation relations (2) and is independent of the choice of concrete representation of the operators $\hat{K}_j$. We also recall that the operators $\hat{K}_j$ satisfy the Jacobi identity $[A, [B, C]] + [B, [C, A]] + [C, [A, B]] = 0$.

For the purposes of this work we choose to express these operators using the annihilation and creation operators $\hat{a}_k, \hat{a}_k^\dagger$ of two harmonic oscillators that satisfy the canonical commutation relations $[\hat{a}_k, \hat{a}_{k'}^\dagger] = \delta_{kk'}$, while all others vanish. Employing these operators we introduce the following expressions:

$$\hat{K}_x = \frac{1}{2}(\hat{a}_1^\dagger \hat{a}_2^\dagger + \hat{a}_1 \hat{a}_2), \quad \hat{K}_y = \frac{i}{2}(\hat{a}_1 \hat{a}_2 - \hat{a}_1^\dagger \hat{a}_2^\dagger),$$

$$\hat{K}_z = \frac{1}{2}(\hat{a}_1^\dagger \hat{a}_1 + \hat{a}_2 \hat{a}_2^\dagger), \quad \hat{N} = \hat{a}_1^\dagger \hat{a}_1 + \hat{a}_2^\dagger \hat{a}_2, \tag{3}$$

which include also the definition of the number operator $\hat{N}$ and we observe that $\hat{K}_z = (\hat{N} + 1)/2$. The Casimir invariant for this Lie algebra is $\hat{K}^2 := \hat{K}_z^2 - \hat{K}_x^2 - \hat{K}_y^2$ and satisfies $[\hat{K}^2, \hat{K}_j] = 0$ for all j. Note that $\hat{K}_z$ is the only element of the group that commutes with the number operator $\hat{N}$. This feature is key, as we see below.

An equivalent form of the unitary operator introduced in (1) is given by

$$\hat{U}_{su} = e^{i\theta\hat{K}_z} e^{i\chi\hat{K}_y} e^{-i\theta\hat{K}_z}, \tag{4}$$

where the parameters θ and χ can be determined as functions of ζ and ϕ by means of the following relations:

$$\cos(\theta(\zeta, \phi)) = \frac{\sin \phi}{\sqrt{\sin^2 \phi + (1 - \cos \phi)^2 \cosh^2 \zeta}},$$

$$\cosh(\chi(\zeta, \phi)) = (1 - \cos \phi) \cosh^2 \zeta + \cos \phi, \qquad (5)$$

which have already been obtained in the literature [46].

The form of expression (4) of the unitary operator $\hat{U}_{su}$ dramatically simplifies the computation of the average values of any observable that commutes with $\hat{K}_z$. To see this, consider a state diagonal in the Hamiltonian eigenbasis as initial state $|\text{in}\rangle$ (as will always be in this work) and the final state $|\text{out}\rangle$ at the end of the interference process. Then, we can easily compute the average number $N_{\text{out}} := \langle \text{out}|\hat{N}|\text{out}\rangle$ of particles leaving the interferometer, and we find

$$
\begin{aligned}
N_{\text{out}} &= \langle \text{in}|\hat{U}_{su}^\dagger \hat{N} \hat{U}_{su}|\text{in}\rangle \\
&= \langle \text{in}|e^{i\theta \hat{K}_z} e^{-i\chi \hat{K}_y} \hat{N} e^{i\chi \hat{K}_y} e^{-i\theta \hat{K}_z}|\text{in}\rangle \\
&= (N_{\text{in}} + 1) \cosh \chi - 1, \qquad (6)
\end{aligned}
$$

where $N_{\text{in}} := \langle \text{in}|\hat{N}|\text{in}\rangle$ is the average number of particles entering the interferometer. It is not surprising that the number of additional particles created is determined ultimately by the squeezing parameter χ, since squeezing introduces energy into the system and therefore potentially new excitations.

B. Phase sensitivity

Quantum metrology studies the precision that can be obtained by measurements of physical parameters when quantum resources can be exploited [58,59]. Among possible applications one finds precision measurements using interferometers, where the performance of the interferometer can be evaluated by estimating its phase sensitivity [60]. This is the precision with which we can discriminate the variation of an observable $\hat{O}(\phi)$ due to the modulation of an internal parameter ϕ [61]. At the output of the interferometer the average value $O(\phi) := \langle \hat{O}(\phi) \rangle_{\hat{\rho}}$ of the observable $\hat{O}(\phi)$ in the state $\hat{\rho}$ will depend on ϕ. A small shift $\delta\phi$ of the variable ϕ induces a change $\delta O = O(\phi + \delta\phi) - O(\phi) = \frac{\partial O(\phi)}{\partial \phi} \delta\phi$, to first order in $\delta\phi$. To make sure that the variation of the observable is only due to the modulation of ϕ, the variation itself must be at least as large as the statistical fluctuation of the observable itself, which translates in the condition $\delta O = \Delta O$, where ΔX determines the standard deviation of the quantity X. This means that

$$\delta\phi = \frac{\Delta O}{\left| \frac{\partial O(\phi)}{\partial \phi} \right|} \qquad (7)$$

is the variation of ϕ determining the smallest appreciable perturbation of O beyond its statistical fluctuation. Note that an observable undergoing a Poissonian fluctuation achieves its best sensitivity at

$$\Delta\phi_{\text{SNL}} = 1/\sqrt{N_\phi}, \qquad (8)$$

which is called *shot-noise limit* (SNL) and is the maximum precision achieved by a Mach-Zehnder interferometer when the two input channels are seeded by a coherent state [59]. In Eq. (8) the quantity N_ϕ indicates the number of photons
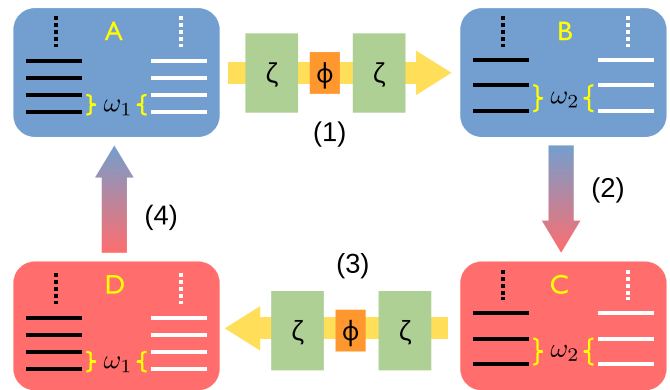

FIG. 2. Pictorial representation of two degenerate quantum harmonic oscillators performing the $SU(1, 1)$ Otto cycle. The four stages labeled by the capitol letters are connected by the four strokes of the cycle. In particular: (1) $SU(1, 1)$ adiabatic compression $(A \rightarrow B)$, (2) $SU(1, 1)$ hot isochoric transformation $(B \rightarrow C)$, (3) $SU(1, 1)$ adiabatic expansion transformation $(C \rightarrow D)$, and (4) cold isochoric $(D \rightarrow A)$.

undergoing the phase shift. A Mach-Zehnder interferometer overcoming this limit means therefore taking advantage of the sub-Poissonian (nonclassical) statistics of the input state to perform high-precision measurements of δO. For instance, it was shown [58,62] that the phase sensitivity can scale as $\Delta\phi_{\text{HL}} = 1/N_\phi$ if both input channels of the Mach-Zehnder interferometer are seeded with squeezed light. The scaling proportional to N_ϕ^{-1} is also called the *Heisenberg limit* (HL) since it is strictly connected to the energy-time uncertainty principle [63]

$$\Delta N \Delta\phi \geqslant 1. \qquad (9)$$

The crucial advantage of using the $SU(1, 1)$ interferometer is the fact that it can overcome the SNL without requiring any exotic input state. In particular, it has been demonstrated that the precision of such interferometer can reach the Heisenberg limit by seeding it with the vacuum state [46].

III. MODEL OF A $SU(1, 1)$ HEAT ENGINE

The system of interest is depicted in Fig. 2 and consists of two degenerate bosonic modes (i.e., with the same frequency), which are employed as working substance and undergo an Otto cycle. The Otto cycle is a four-stroke cycle in which the working substance undergoes four transformations:

(1) *adiabatic compression*, during which the two oscillators, decoupled from any bath, increase their frequency;

(2) *hot isochoric* thermalization of the system with a hot bath at temperature T_h once the compression stops;

(3) *adiabatic expansion*, during which the two oscillators release output work; their frequency returns to the same value that they had at the beginning of stage (1);

(4) *cold isochoric*, during which the system thermalizes with the cold bath at temperature T_c and is ready to repeat the cycle.

Note that during each isochoric transformation the system is weakly coupled to the baths, which ensures that the

dressing of the bare system Hamiltonian, due to the presence of nonvanishing system-bath interactions, can be ignored [64].

The frequency variation at each adiabatic transformation occurs by means of a unitary evolution operator $\hat{U}(t)$ defined in the next section. This operator encodes the information about the two protocols controlling both the time dependence of the bare frequency of the oscillators (which is identical) and the strength of their interaction. The unitary evolution operator varies according to the transformation it is referred to the following: during compression, the frequencies are increased, whereas they decrease during the expansion. Crucially, we see that the average values $O(t) := \langle \hat{U}^\dagger(t)\hat{O}\hat{U}(t)\rangle_{\hat{\rho}}$ in the state $\hat{\rho}$ of any observable $\hat{O}$ of interest at the end of the time evolution are indistinguishable from its average value after the unitary transformation determined by Eq. (4).

A. Time evolution operator and Hamiltonian

We assume that the adiabatic transformations causing the frequency shift of the two oscillators is represented by the following, already time-ordered, unitary operator:

$$\hat{U}(t) := \overleftarrow{\mathcal{T}}e^{-i\int_0^t dt'\hat{H}_S(t')} = e^{-if_z(t)\hat{K}_z}e^{-if_y(t)\hat{K}_y}, \quad (10)$$

where $f_z(t)$ and $f_y(t)$ are two time-dependent functions encoding the protocols of each adiabatic transformations. In our notation, we set $\hbar = 1$. Since the time evolution operator must be the identity operator $\mathbb{1}$ at $t = 0$, these two functions are subject to the initial conditions $f_z(0) = f_y(0) = 0$. The Hamiltonian written in the Schrödinger picture inducing such time evolution is obtained from Eq. (10) by taking the time derivative on both sides and then multiplying each side by $\hat{U}^\dagger(t)$ on the right [65]. We find

$$\hat{H}_S(t) = \dot{f}_z(t)\hat{K}_z + \dot{f}_y(t)[\cos(f_z(t))\hat{K}_y - \sin(f_z(t))\hat{K}_x]. \quad (11)$$

We want the two oscillators to be decoupled at the beginning of each adiabatic transformation. In this way, the system can thermalize at each isochoric transformation without the two subsystems interacting. This means that, at $t = 0$, we require $\dot{f}_y(0) = 0$, and the initial Hamiltonian $\hat{H}_S(0)$ reduces to

$$\hat{H}_S(0) = \dot{f}_z(0)\hat{K}_z = \frac{\dot{f}_z(0)}{2}(\hat{a}_1^\dagger \hat{a}_1 + \hat{a}_2^\dagger \hat{a}_2 + 1). \quad (12)$$

This allows us to attribute the following initial conditions to the time derivative: $\dot{f}_z(0) = 2\omega(0) = 2\omega_i$, where ω_i is the frequency of the two oscillators before the time evolution. Importantly, at the end of the dynamics, that is at time $t = t_f$, we re-initialize the Hamiltonian; thus, $\hat{H}_S(t_f) = \hat{H}_S(0)$. This adds the following further boundary condition $\dot{f}_y(t_f) = 0$:

The Hamiltonian $\hat{H}_H(t)$ in the Heisenberg picture is obtained from Eq. (10) via the relation

$$\hat{H}_H(t) := \hat{U}^\dagger(t)\hat{H}_S(0)\hat{U}(t) \equiv -i\frac{d\hat{U}^\dagger(t)}{dt}\hat{U}(t), \quad (13)$$

and it reads

$$\hat{H}_H(t) = 2\omega(t)[\text{ch}(f_y(t))\hat{K}_z - \text{sh}(f_y(t))\hat{K}_x] + \dot{f}_y(t)\hat{K}_y, \quad (14)$$

where we identified $\dot{f}_z(t) = 2\omega(t)$, and we have introduced $\text{ch}(x) := \cosh x$ and $\text{sh}(x) := \sinh x$ for simplicity of notation.

Note that if we had $\dot{f}_y(t) \approx 0$ at all times we would have $f_y(t) \approx 0$ due to the initial conditions, and the time evolution would describe a quantum adiabatic transformation [8]. Once the dynamics stops at time t_f, the Hamiltonian $\hat{H}_H(t)$ becomes

$$\hat{H}_H(t_f) = 2\omega_f[\text{ch}(f_y(t_f))\hat{K}_z - \text{sh}(f_y(t_f))\hat{K}_x], \quad (15)$$

where $\omega_f \equiv \omega(t_f)$ is the frequency of the two oscillators at the end of the dynamics. The relation between the initial and final frequencies is $\omega_f > \omega_i$ at the end of the adiabatic compression, and $\omega_f < \omega_i$ at the end of the adiabatic expansion.

B. The SU(1, 1) adiabatic transformation

We now show that, although the unitary operator in Eq. (10) driving the adiabatic transformation does not perfectly match the unitary operator of the SU(1, 1) interferometer in Eq. (4) (a second phase shift misses), the average values of any observable at the end of each adiabatic transformation are indistinguishable from the average values obtained as result of both the frequency tuning and the SU(1, 1) interference of the bosonic modes.

Recall that the thermal state, which is the state of the two oscillators at the beginning of each adiabatic transformation, is a mixed state defined as $\rho = e^{-\beta\hat{H}_S(0)}/Z$, where Z is the partition function and $\beta = 1/(k_B T)$, with T representing temperature and k_B being the Boltzmann constant. In our case, since

$$\hat{H}_S(0) = 2\omega_i\hat{K}_z, \quad (16)$$

and

$$2\hat{K}_z = \hat{N} + 1 = \hat{a}_1^\dagger \hat{a}_1 + \hat{a}_2^\dagger \hat{a}_2 + 1, \quad (17)$$

we have

$$\hat{\rho} = \sum_{n_1}\sum_{n_2}\frac{e^{-\omega_i\beta(n_1+n_2+1)}}{Z}|n_1, n_2\rangle\langle n_1, n_2|, \quad (18)$$

where in the last line we expressed the thermal state in terms of the Hamiltonian (Fock) eigenstates. The partition function $Z := \text{Tr}(\hat{\rho})$ therefore reads

$$Z = \sum_{n_1}\sum_{n_2}e^{-\omega_i\beta(n_1+n_2+1)} = [2\sinh(\beta\omega_i/2)]^{-2}. \quad (19)$$

Note that $\hat{K}_z$ and the Hamiltonian at $t = 0$ share the same eigenbasis, because they commute. This means that, at the end of the interference process described by the unitary transformation in Eq. (4), the average value $O_H := \langle\hat{O}_H\rangle_{\hat{\rho}} \equiv \text{Tr}[\hat{O}_H\hat{\rho}]$ of any observable $\hat{O}_H$ calculated with respect to this thermal state must be of the form

$$\begin{aligned} O_H &= \text{Tr}[\hat{U}_{su}^\dagger\hat{O}_S\hat{U}_{su}\hat{\rho}] \\ &= \text{Tr}[e^{i\theta\hat{K}_z}e^{-i\chi\hat{K}_y}e^{-i\theta\hat{K}_z}\hat{O}_S e^{i\theta\hat{K}_z}e^{i\chi\hat{K}_y}e^{-i\theta\hat{K}_z}\hat{\rho}] \\ &= \text{Tr}[e^{-i\chi\hat{K}_y}e^{-i\theta\hat{K}_z}\hat{O}_S e^{i\theta\hat{K}_z}e^{i\chi\hat{K}_y}\hat{\rho}], \end{aligned} \quad (20)$$

where in the last step we took advantage of the commutation between $\hat{K}_z$ and $\hat{\rho}$, as well as the cyclic property of the trace. The average value of $\hat{O}_H$ at the end of the interference process would therefore be indistinguishable from its average value at time t_f if the time evolution is governed by the unitary operator

in Eq. (10), assuming $\chi = -f_y(t_f)$ and $\theta = -2\int_0^{t_f} dt'\omega(t') = -f_z(t_f)$:

$$O_H = \text{Tr}[\hat{U}_{su}^\dagger \hat{O}_S \hat{U}_{su}\hat{\rho}] = \text{Tr}[\hat{U}^\dagger(t)\hat{O}_S\hat{U}(t)\hat{\rho}]. \quad (21)$$

This proves that the average values of a observable calculated after the adiabatic transformation controlled via $\hat{U}(t)$ corresponds to the average value of the same observable when the system undergoes both the frequency tuning and the SU(1, 1) interference process. As a consequence of these considerations we wish to strongly emphasize the fact that controlling the protocol functions at the end of the dynamics, $f_y(t_f)$ and $f_z(t_f)$, means controlling χ and θ, which allows us to directly manipulate both the squeezing parameter ζ and the phase ϕ of the equivalent SU(1, 1) interferometer by means of the constituent relations (5).

In the study of the performance of the thermodynamic cycle presented here we note that the only observable of interest is the Hamiltonian, whose average value gives the amount of energy of the system at each step of the cycle. Employing Eqs. (3), (15), and (18)–(20) we finally obtain

$$\langle \hat{H}_H(t_f)\rangle_{\hat{\rho}} = \omega_f \cosh \chi \coth\left(\frac{\beta\omega_i}{2}\right). \quad (22)$$

IV. ANALYTICAL RESULTS

We have introduced the working substance and the functioning of the SU(1, 1) adiabatic transformation. Therefore, we can now discuss the performance of the quantum heat engine. In particular, we focus on the efficiency of the Otto cycle and the phase sensitivity of the equivalent SU(1, 1) interferometer at the end of the adiabatic expansion. Interestingly, we see that it is possible to find a regime of parameters wherein our system can work simultaneously as a quantum heat engine producing net work, and as an SU(1, 1) interferometer with precision beyond the standard quantum limit. Finally, we discuss an application of our model of SU(1, 1) heat engine in the context of circuit QED [66].

A. Thermodynamic cycle

In this section we study the efficiency of the heat engine. Therefore, we start from calculating the average value of the energy at each of the four stages of the cycle. To do this, we calculate the average value of the Hamiltonian at the end of the two thermalization branches (isochoric transformation) and at the end of the two adiabats:

$$\langle \hat{H}\rangle_A = \omega_1 \coth\left(\frac{\beta_c\omega_1}{2}\right), \quad (23)$$

$$\langle \hat{H}\rangle_B = \omega_2 \cosh \chi \coth\left(\frac{\beta_c\omega_1}{2}\right), \quad (24)$$

$$\langle \hat{H}\rangle_C = \omega_2 \coth\left(\frac{\beta_h\omega_2}{2}\right), \quad (25)$$

$$\langle \hat{H}\rangle_D = \omega_1 \cosh \chi \coth\left(\frac{\beta_h\omega_2}{2}\right), \quad (26)$$

where ω_1 and ω_2 are the oscillators frequency at the beginning and at the end of the compression, respectively, whereas $\beta_h = 1/(k_B T_h)$ and $\beta_c = 1/(k_B T_c)$ are the inverse temperatures of

the hot and cold baths, respectively. Here k_B is the Boltzmann constant as usual.

From these expressions, we can calculate the average work and heat transferred during each transformation. During the adiabatic compression, the external work done on the system is given by $W_{AB} := \langle \hat{H}\rangle_B - \langle \hat{H}\rangle_A$, which becomes

$$\frac{W_{AB}}{\omega_1} = \left(\frac{\omega_2}{\omega_1}\cosh \chi - 1\right)\coth\left(\frac{\beta_c\omega_1}{2}\right). \quad (27)$$

The system is then thermalized to the hot bath absorbing the amount $Q_{BC} = \langle \hat{H}\rangle_C - \langle \hat{H}\rangle_B$ of heat from the environment, given by

$$\frac{Q_{BC}}{\omega_2} = \coth\left(\frac{\beta_h\omega_2}{2}\right) - \cosh \chi \coth\left(\frac{\beta_c\omega_1}{2}\right). \quad (28)$$

At this point, the system releases energy in the form of fruitful work defined by $W_{CD} = \langle \hat{H}\rangle_D - \langle \hat{H}\rangle_C$. We find

$$\frac{W_{CD}}{\omega_2} = \left(\frac{\omega_1}{\omega_2}\cosh \chi - 1\right)\coth\left(\frac{\beta_h\omega_2}{2}\right). \quad (29)$$

Notice that W_{AB} can be obtained from W_{CD} by exchanging the two frequencies (and vice versa), as well as the hot and cold temperatures.

Finally, the system thermalizes with the cold bath ceding heat to the environment defined by $Q_{DA} := \langle \hat{H}\rangle_A - \langle \hat{H}\rangle_D$, which reads

$$\frac{Q_{DA}}{\omega_1} = \coth\left(\frac{\beta_c\omega_1}{2}\right) - \cosh \chi \coth\left(\frac{\beta_h\omega_2}{2}\right). \quad (30)$$

The cycle can therefore restart from the compression stage $A \to B$.

The explicit expressions obtained above allow us to calculate the efficiency of the cycle. This is defined as the ratio between the net work and the heat absorbed by the system. We employ Eqs. (27)–(29) to obtain $\eta = -(W_{AB} + W_{CD})/Q_{BC}$, which for us reads

$$\eta = 1 - \frac{\omega_1}{\omega_2}\frac{\cosh \chi \coth\left(\frac{\beta_h\omega_2}{2}\right) - \coth\left(\frac{\beta_c\omega_1}{2}\right)}{\coth\left(\frac{\beta_h\omega_2}{2}\right) - \cosh \chi \coth\left(\frac{\beta_c\omega_1}{2}\right)}. \quad (31)$$

This result, unsurprisingly, is very similar to what achieved in the literature [39], where the coefficients Q_1^* and Q_2^*, in the same manner of our parameter χ, encode the adiabaticity of the compression and the expansion, respectively. Consequently, an analysis of the output power (which also includes the study of the efficiency at maximum power) would not substantially differ from what accomplished before [39], and therefore we choose not to report it here.

The squeezing during each adiabatic process causes the presence of quantum friction. This quantity can be computed as described in Ref. [45]. In our case, it is given by $W_{fric} = W_{CD} - W_{ad}$, which explicitly reads

$$W_{fric} = 2\omega_1 \sinh^2(\chi/2)\coth\left(\frac{\beta_h\omega_2}{2}\right). \quad (32)$$

Here, the work exchanged during the expansion, assuming the process were quantum adiabatic, is given by

$$W_{ad} = (\omega_1 - \omega_2)\coth\left(\frac{\beta_h\omega_2}{2}\right). \quad (33)$$

Evidently, the higher the parameter χ, the smaller the amount of energy extracted from the system during the expansion. In general, in order for our system to work as quantum heat engine we require $-(W_{AB} + W_{CD}) > 0$, or $\chi < \chi_{\max}$, where we have defined $\chi_{\max}$ through

$$\cosh(\chi_{\max}) < \frac{\omega_1 \coth\left(\frac{\beta_c \omega_1}{2}\right) + \omega_2 \coth\left(\frac{\beta_h \omega_2}{2}\right)}{\omega_2 \coth\left(\frac{\beta_c \omega_1}{2}\right) + \omega_1 \coth\left(\frac{\beta_h \omega_2}{2}\right)}. \quad (34)$$

Interestingly, if $k_B T_h \ll \hbar\omega_2$ and $k_B T_c \ll \hbar\omega_1$, we have $\coth(\beta_c \omega_1/2) \approx 2T_c/\omega_1$ and $\coth(\beta_h \omega_2/2) \approx 2T_h/\omega_2$, and we can express the positive work condition in terms of the temperature ratio as

$$\frac{T_h}{T_c} > \frac{\omega_2}{\omega_1} \frac{\omega_2 \cosh\chi - \omega_1}{\omega_2 - \omega_1 \cosh\chi}. \quad (35)$$

As expected, the right side of the equation above reduces to the frequency ratio ω_2/ω_1 in case of quantum adiabatic transformations, $\chi = 0$.

Note that Eq. (34) corresponds to an upper bound for the parameter χ. Nevertheless, this bound does not necessarily affect our choice of the squeezing parameter ζ. From Eq. (5), we see that we can choose relatively large ζ at the price of a narrower range for ϕ. With ζ fixed, we can easily find that the phase takes values in the interval $0 \leqslant \phi < \phi_{\max}$, where $\phi_{\max}$ is defined as

$$\cos(\phi_{\max}(\zeta)) = 1 - 2 \frac{\sinh^2(\chi_{\max}/2)}{\sinh^2 \zeta}. \quad (36)$$

Notably, the higher ζ the more $\phi_{\max}$ tends to vanish.

Before concluding this section, we find it useful to elaborate on the importance of having two interacting oscillators evolving according to Eq. (10), rather than a single oscillator as the working substance performing finite time transformations. We recall that it is indeed possible to extract power from a single harmonic oscillator experiencing nonadiabaticity during the adiabatic strokes [39]. Likewise, in the case of our quantum system, the Hamiltonian of a single quantum harmonic oscillator with a time-dependent frequency can be expressed in terms of elements of the $\mathfrak{su}(1,1)$ Lie algebra given in Eq. (3) [67]. This suggests that rapidly tuning the frequency of a single quantum harmonic oscillator during any adiabatic stroke induces a squeezing effect on the quantum state. Therefore, the squeezing effect is the price paid in terms of quantum friction to generate power from a single oscillator, corresponding to energy wasted by the engine.

Given that the squeezing of the quantum state is an inevitable consequence of rapidly tuning the frequency of quantum harmonic oscillators, with our model of QHE we intend to take advantage of this effect to better estimate the expectation value of the energy exchange with the system. The action of the two protocols (guiding both the frequencies and the coupling parameter of the oscillators, rather than relying on a single protocol) enables better control of the squeezing effect and allows us to exploit the inner friction as a quantum metrological tool.

B. Efficiency at minimum sensitivity

It should be clear from Sec. III B that we can interpret the final stage of any adiabatic strokes of the quantum heat engine as an interference process. The parameters θ and χ, representing the protocols of the time evolution operators at t_f, can be parametrized in terms of the squeezing parameter ζ and the internal phase ϕ of a SU(1, 1) interferometer by means of Eq. (5).

Assuming that the adiabatic processes induce an amount of squeezing quantified by ζ, and that the source of instability in our protocols is entirely captured by the phase ϕ, we can then ask what precision we can achieve from the knowledge of an observable parametrically dependent on ϕ and subject to thermal noise.

In other words, since θ and χ are connected to the protocols of the QHE at the end of the adiabats, we may ask how precisely we can attribute the uncertainty of an observable to the instability of $f_z(t_f)$ and $f_y(t_f)$, rather than to its own thermal fluctuation.

Using the mathematical tools introduced in Sec. II B, we can make use of the phase sensitivity to test the precision of our knowledge of relevant observables, such as the output number of particles or, more importantly, the average energy at the end of the process.

Note that, although the study of work fluctuations has a fundamental role in quantum thermodynamics [68,69], work is not an observable [70,71], but it is calculated as the difference between the average energy of the working substance after the adiabatic transformation (which depends on the internal phase of the interferometer) and the average energy before the adiabatic transformation (which does not depend on the phase ϕ). For these reasons, we discuss only those observables which are directly involved by the variation of ϕ in our study of the phase sensitivity.

According to the definition in Eq. (7), we need to calculate both the variance of our observables and their derivative with respect to φ. Focusing on the adiabatic expansion (which is more affected by thermal fluctuations), we compute $\Delta^2 N = \text{Tr}[N_H^2 \rho] - \text{Tr}[N_H \rho]^2$ and $\Delta^2 H = \text{Tr}[H_H^2 \rho] - \text{Tr}[H_H \rho]^2$, which read

$$\Delta^2 N = \frac{1}{2}\left[\cosh(2\chi)\coth^2\left(\frac{\beta_h \omega_2}{2}\right) - 1\right], \quad (37)$$

$$\Delta^2 H = 2\omega_1^2 \left\{ \Delta^2 N + \frac{1}{4}\left[\coth^2\left(\frac{\beta_h \omega_2}{2}\right) + 1\right] \right\}, \quad (38)$$

whereas the latter are

$$\frac{\partial N_H}{\partial \phi} = \sin\phi \sinh^2\zeta \coth^2\left(\frac{\beta_h \omega_2}{2}\right), \quad (39)$$

$$\frac{\partial H_H}{\partial \phi} = \omega_1 \frac{\partial N_H}{\partial \phi}. \quad (40)$$

Clearly, both variance and derivative depend on the phase of the interferometer ϕ. We notice that the variance of the energy is not proportional to ΔN, which is due to the fact that the Hamiltonian operator also includes the energy of the quantum vacuum.

The two phase sensitivity curves are plotted in Fig. 3, along with the efficiency of the thermodynamic cycle in Eq. (43), with respect to the phase ϕ. Here, the indices "N" and "H" indicate the phase sensitivity calculated with respect to the excitation number and the Hamiltonian, respectively. We normalized the curves with respect to natural benchmarks: the
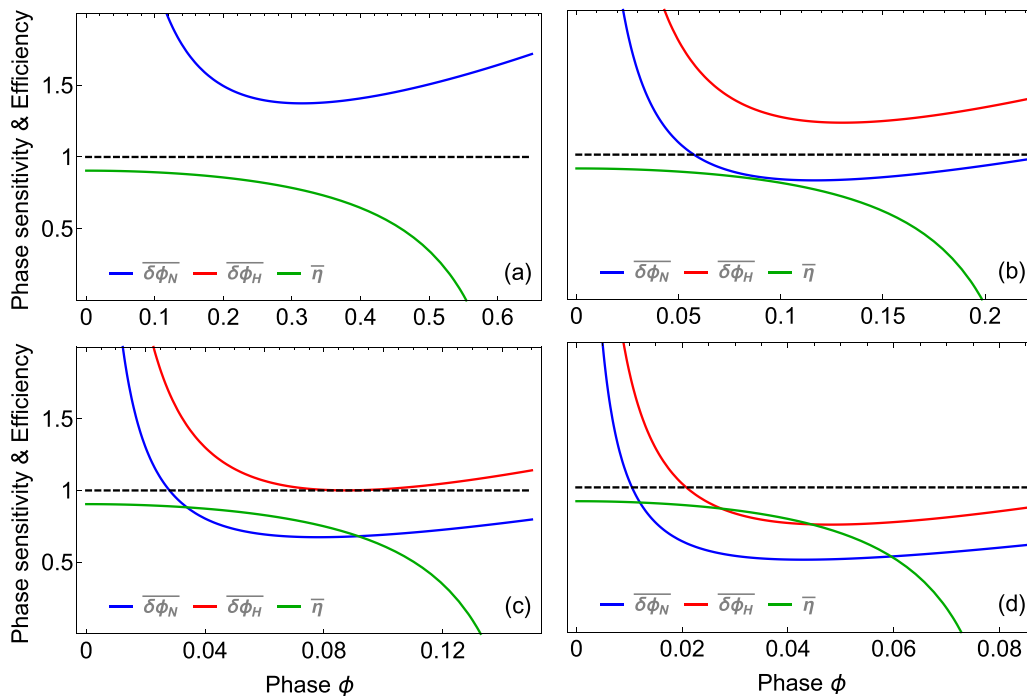
FIG. 3. Normalized phase sensitivity calculated with respect to the average excitation number (blue curve) and the average energy (red curve), normalized efficiency of the Otto cycle (magenta curve). The bar above all quantities in the legend stresses these normalization. The dashed black horizontal line indicates the normalization. The four panels refer to different squeezing intensities: (a) $\zeta = 2$, (b) $\zeta = 3$, (c) $\zeta = 3.4$, and (d) $\zeta = 4$. Other parameters are $\omega_1 = 0.1$, $\omega_2 = 1$, $T_h = 2$, and $T_c = 0.01$. Frequencies and temperatures are normalized with respect to ω_2.

phase sensitivity is normalized with respect to the SNL, while the efficiency is normalized with respect to the Carnot limit $\eta_C = 1 - T_c/T_h$.

Recall that the SU(1, 1) interferometer consists of active elements that do not preserve the number of particles. For this reason, in the definition of SNL in Eq. (8) we need the actual number of particles subject to the phase modulation. We therefore have $\Delta\phi_{SNL} = 1/\sqrt{N_\phi}$, where

$$N_\phi = (N_{in} + 1)\cosh\zeta - 1. \tag{41}$$

At $\phi = 0$ we have $\chi = 0$, and the quantum system performs quantum adiabatic transformations reaching therefore the efficiency of an ideal Otto cycle $\eta_O = 1 - \omega_1/\omega_2$ [8]. As soon as we increase the phase ϕ, the efficiency inevitably decreases due to the inner friction until it vanishes at ϕ_{max}. Note that, as predicted in Eq. (36), the operational phase range of our quantum system as a heat engine decreases with increasing squeezing ζ.

We now look at the two phase sensitivity curves. We observe that, as the squeezing parameter ζ increases, the phase sensitivity decreases. For very large values of ζ, both curves reach their minimum values below the SNL line (indicated by the black dotted line in the graph). In this regime, our quantum system functions both as a quantum heat engine and as SU(1, 1) interferometer working beyond the classical limit.

In quantum metrology, the range of ϕ where the phase sensitivity overcomes the SNL, i.e., $\delta\phi < \Delta\phi_{SNL}$, is sometimes called supersensitivity [50,57,72]. Evidently, the supersensitivity range depends on the observable with respect to which

the phase sensitivity is calculated: from Figs. 3(b)–3(d), we see that, for a fixed squeezing parameter ζ, $\delta\phi_N$ is always lower than $\delta\phi_H$, and the corresponding supersensitivity range is larger. Note that, due to the energy-time uncertainty principle [as expressed in Eq. (9)], improving the phase sensitivity requires a large number of excitations in the phase shifter. This is why we simulate the SU(1,1) interference processes with high squeezing parameters (see Fig. 3). The first squeezing process creates a large number of excitations. These excitations undergo phase shifting and, finally, antisqueezing occurs. However, despite the large number of particles created and annihilated in the squeezing processes, the total squeezing-phase-(anti-)squeezing operation generates few excitations. This explains why the system can properly work as a QHE.

At this point, we may be interested at the efficiency of the cycle when the minimum of the phase sensitivity $\Delta\phi_H$ reaches the SNL. To calculate this quantity, we first need to calculate the minimum ζ required to reach the SNL. Given a set of $\{\omega_1, \omega_2, T_h, T_c\}$ of frequencies and temperatures, this value determines the minimum amount of squeezing necessary for the phase sensitivity to reach the SNL in at least one point of the phase ϕ, which we call ϕ_{SNL}:

$$\delta\phi_{min}(\zeta_{SNL}) = \Delta\phi_{SNL}. \tag{42}$$

The corresponding phase ϕ_{SNL} is obtained from Eq. (42) and used to calculate the efficiency at the SNL. This reads

$$\eta = 1 - \frac{\omega_1}{\omega_2} \frac{\cosh\chi_{SNL}\coth\left(\frac{\beta_h\omega_2}{2}\right) - \coth\left(\frac{\beta_c\omega_1}{2}\right)}{\coth\left(\frac{\beta_h\omega_2}{2}\right) - \cosh\chi_{SNL}\coth\left(\frac{\beta_c\omega_1}{2}\right)}, \tag{43}$$
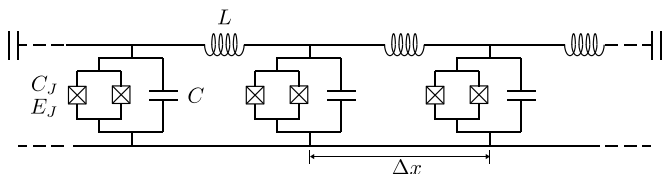
FIG. 4. Example of platform supporting the SU(1, 1) Otto cycle. The superconducting transmission line consists of a series of inductors, while two consecutive inductors are connected by a node with a SQUID and a capacitor, placed in parallel [87,88].

where $\chi_{\text{SNL}} \equiv \chi(\zeta_{\text{SNL}}, \phi_{\text{SNL}})$. These quantities are not simple to calculate analytically. However, we numerically computed both ζ_{SNL} and η_{SNL} with the choice of parameters used in Fig. 3. This result in $\zeta_{\text{SNL}} = 3.4$ and $\eta_{\text{SNL}} \simeq 0.705$. For completeness, we also report the efficiency at $\phi = 0$, $\eta_{\text{O}} = 0.9$, and the Carnot efficiency, $\eta_{\text{C}} = 0.995$.

C. Application to superconducting transmission lines

The specific dynamics described by the unitary time evolution operator in Eq. (10) can be achieved in circuit QED [73,74]. Thanks to their flexibility and high controllability, superconducting circuits are indeed promising platforms for the realization of QHE [75–82]. Moreover, transmission lines simulating particle creation phenomena [73], such as the dynamical Casimir effect [83–85], have already been taken into account for the study of effects of quantum friction on the efficiency of the Otto cycle [86].

Here we consider the device drawn in Fig. 4 and discussed in detail in Refs. [87,88] as a possible platform for the implementation of the SU(1, 1) Otto cycle proposed here. The transmission line is based on a series of unit cells. Each cell consists of a inductor placed in series, and a superconducting quantum interference device (SQUID) placed in parallel. Finally, each SQUID is parallel to a capacitor.

This transmission line has been proposed as a platform to simulate the cosmological model of particle creation due to a rapid expansion of the space-time [87,89,90]. The Lagrangian, as well as the equations of motion, describing the quantum magnetic flux field along the transmission line can indeed be interpreted as a $(1 + 1)$-dimensional equivalent of the Lagrangian of a quantum massive scalar field immersed in a dynamical background described by a time-dependent Friedmann-Robertson-Walker metric [89,90]. It emerges that the modes of the quantum magnetic flux undergo the same Bogoliubov transformations leading to the squeezing of the quantum vacuum of the scalar field before the expansion process.

For later convenience, we report here the dispersion relation of the transmission line, as well as the Bogoliubov transformations. The former has already been obtained [87,91] and reads

$$\omega_j(t) = \sqrt{\frac{4 \sin^2\left(\frac{k_j \Delta x}{2}\right)}{LC} + \left(\frac{2\pi}{\Phi_0}\right)^2 \frac{E(t)}{C}}, \qquad (44)$$

where $k_j = 2\pi j/(N_{\text{cell}} \Delta x)$ are the wave vectors of the quantum field assuming to possess a transmission line with N_{cell} cells, Δx is the cell length, L and C are respectively the

inductance and the effective capacitance of the transmission line, Φ_0 is the magnetic flux quantum, and $E(t) = E_0[A \pm B \tanh(\nu t)]$ is the time-dependent Josephson energy, with A and B adimensional constants and ν the rapidity coefficient. The sign in the Josephson energy depends on the thermodynamic transformation we are considering: the positive sign refers to the frequency during the adiabatic compression, while the negative sign refers to the expansion [92]. The Bogoliubov transformations have the general expression

$$\hat{a}_j^{\text{out}} = \alpha_j \hat{a}_j^{\text{in}} + \beta_j^* \left(\hat{a}_{-j}^{\text{in}}\right)^\dagger, \qquad (45)$$

which is well known in the literature [87,89,90], while the Bogoliubov coefficients α_j, β_j for this particular case read

$$\alpha_j = \left(\frac{\omega_f}{\omega_i}\right)^{\frac{1}{2}} \frac{\Gamma(1 - i\omega_i/\nu)\Gamma(-i\omega_f/\nu)}{\Gamma(-i\omega_+/\nu)\Gamma(1 - i\omega_+/\nu)},$$

$$\beta_j = \left(\frac{\omega_f}{\omega_i}\right)^{\frac{1}{2}} \frac{\Gamma(1 - i\omega_i/\nu)\Gamma(i\omega_f/\nu)}{\Gamma(i\omega_-/\nu)\Gamma(1 + i\omega_-/\nu)}. \qquad (46)$$

Here, we define $\omega_i \equiv \omega_j(t \to -\infty)$ and $\omega_f \equiv \omega_j(t \to +\infty)$ as the frequencies of the degenerate modes before and after the transformation, respectively. Additionally, $\omega_+ = \omega_i + \omega_f$ and $\omega_- = \omega_f - \omega_i$.

We can safely isolate any degenerate mode pair of the transmission line by properly fixing the boundary conditions of the magnetic flux field. Therefore, we can omit the index j, focus our attention on the first mode pair, and write the Hamiltonian at the beginning of the dynamics as

$$\hat{H}_{\text{S}} = \omega_i\left[\left(\hat{a}_1^{\text{in}}\right)^\dagger \hat{a}_1^{\text{in}} + \left(\hat{a}_2^{\text{in}}\right)^\dagger \hat{a}_2^{\text{in}} + 1\right]. \qquad (47)$$

Note that the two modes are distinguishable, thus *degenerate*. At the end of the dynamics, the Hamiltonian in the Heisenberg picture is

$$\hat{H}_{\text{H}} \equiv \omega_f\left[\left(\hat{a}_1^{\text{out}}\right)^\dagger \hat{a}_1^{\text{out}} + \left(\hat{a}_2^{\text{out}}\right)^\dagger \hat{a}_2^{\text{out}} + 1\right], \qquad (48)$$

which reads

$$\hat{H}_{\text{H}} = (1 + 2|\beta|^2)\left[\left(\hat{a}_1^{\text{in}}\right)^\dagger \hat{a}_1^{\text{in}} + \left(\hat{a}_2^{\text{in}}\right)^\dagger \hat{a}_2^{\text{in}} + 1\right]$$
$$+ 2\text{Re}\{\alpha\beta\}\left[\hat{a}_1^{\text{in}}\hat{a}_2^{\text{in}} + \left(\hat{a}_1^{\text{in}}\right)^\dagger \left(\hat{a}_2^{\text{in}}\right)^\dagger\right]$$
$$+ 2i\text{Im}\{\alpha\beta\}\left[\hat{a}_1^{\text{in}}\hat{a}_2^{\text{in}} - \left(\hat{a}_1^{\text{in}}\right)^\dagger \left(\hat{a}_2^{\text{in}}\right)^\dagger\right] \qquad (49)$$

in terms of the initial operators, and we have used the Bogoliubov identity $|\alpha|^2 - |\beta|^2 = 1$ for this specific one-dimensional degenerate case.

Interestingly for our goals, it turns out that the Bogoliubov transformations in Eq. (45) fulfill the following properties:

(i) they describe a two-mode squeezing scenario;

(ii) they couple two degenerate modes (in the specific case, counterpropagating modes with the same frequency and opposite momentum);

(iii) we can find a regime wherein the Bogoliubov coefficients can take real values.

The first two conditions are evident from Eqs. (45) and (47). However, in order to demonstrate that there is a regime wherein condition (iii) applies (i.e., the last term of Eq. (49) vanishes), in Fig. 5 we plotted the two coupling parameters, namely, the coefficients in the last two lines of Eq. (49), by fixing two convenient values for ω_i and ω_f and varying the
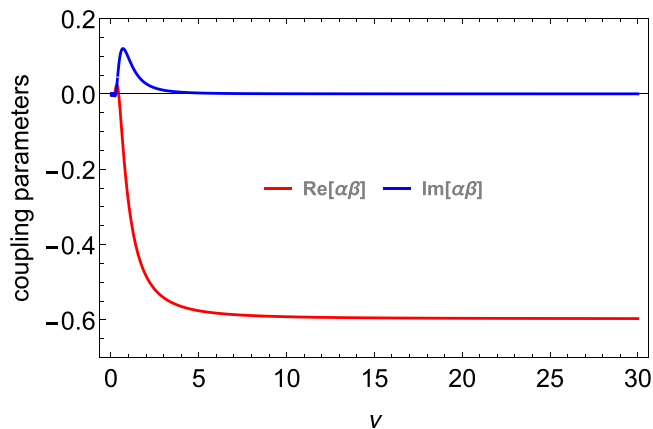
FIG. 5. Dependence of the coupling coefficients $\mathrm{Re}\{\alpha\beta\}$ (red curve) and $\mathrm{Im}\{\alpha\beta\}$ (blue curve) on the parameter ν. When ν is much larger than the two frequencies ω_i and ω_f, the imaginary part of $\alpha\beta$ vanishes. Chosen values: $\omega_\mathrm{i} = 1$ and $\omega_\mathrm{f} = 0.35$. Frequencies and temperatures are normalized with respect to ω_i.

TABLE I. Choice of parameters.

T_h	2 K
T_c	0.01 K
C	0.4 pF
L	60 pH
E_0/C	1 nJ × F^{-1}
N_cell	100
A	1
B	0.78
ν	20

ciency $\overline{\eta} = 0.23$ and the normalized phase sensitivity $\overline{\Delta\phi} = 0.56$ with the choice of parameters reported in Table I.

D. Why the SU(1,1) interferometer?

We believe it is necessary to stress the fundamental role of the $\mathfrak{su}(1, 1)$ Lie algebra employed for the description of the SU(1, 1) interferometer. One may wonder for example if it is possible to realize a similar model of QHE based on other types of interferometers, for instance, on the well-known Mach-Zehnder interferometer. The algebra describing the transformations of the MZI is the $\mathfrak{su}(2)$ Lie algebra, which can be used to describe the rotations in the three-dimensional space [46]. Choosing this interferometer would, however, turn out to be inconvenient: all elements of the $\mathfrak{su}(2)$ Lie algebra commute with the total excitation number operator $\hat{N}$, as can be seen by writing a possible representation $\hat{N} = \hat{a}_1^\dagger \hat{a}_1 + \hat{a}_2^\dagger \hat{a}_2$, $\hat{B}_+ = \hat{a}_1^\dagger \hat{a}_2 + \hat{a}_2^\dagger \hat{a}_1$, and $\hat{B}_- = i(\hat{a}_1^\dagger \hat{a}_2 - \hat{a}_2^\dagger \hat{a}_1)$. This agrees with the well-known property of MZI that preserves the total number of photons injected into the system. This implies that observables of interest for the thermodynamic analysis, such as the Hamiltonian, commute with all elements of the algebra, and are therefore not affected by the Mach-Zehnder unitary transformation. Clearly, we cannot exclude that conceiving a QHE based on more complex algebras can be of any advantage for other purposes. However, here we have chosen to specialize to a QHE based on the SU(1, 1) interference, which introduces great advantages in measuring the observables with precisions that beat the SNL.

rapidity parameter ν. The graph shows that, when ν is much larger than the frequencies of the system, the imaginary part of the coupling constant vanishes, and the Hamiltonian in Eq. (49) corresponds to that in Eq. (15), with $\cosh(f_\mathrm{y}(t_\mathrm{f})) = 1 + 2|\beta|^2$ and $\sinh(f_\mathrm{y}(t_\mathrm{f})) = -2\mathrm{Re}\{\alpha\beta\}$.

Despite the strong analogy between the dynamics in the transmission line and the adiabatic transformation described in this work, we need to clarify an important point. Our model interprets the adiabatic transformation of the Otto cycle as the result of a time evolution that starts at $t = 0$ and terminates at $t = t_\mathrm{f}$. Once the dynamics stops, we control all relevant coefficients at time $t = t_\mathrm{f}$ in order to optimize the phase sensitivity. Instead, the frequency transformation in the transmission line described by the Bogoliubov transformation in Eq. (45) refers to an interaction that occurs in an infinite time, from $t = -\infty$ to $t = +\infty$. The two values of the frequency, ω_i and ω_f, must therefore be intended as the frequencies of the two oscillators in the past and in the future, respectively, as defined below Eq. (45). Nevertheless, if the transition between the two values happens in a short time (or alternatively, if $\nu \gg \omega_\mathrm{i}, \omega_\mathrm{f}$), we can make the reasonable assumption that the adiabatic transformation occurs in a finite time, and that the frequency of the two oscillators in the past and in the future are respectively the effective initial and final frequency of the two oscillators. Moreover, at $t_\mathrm{f} \gg 1/\nu$, namely, at time t far from the frequency transition, we can safely assume that ω_f is constant. This means that the parameter θ approximately takes the value $\theta \approx -\omega_\mathrm{f} t_\mathrm{f}$.

Recalling that $\chi \equiv -f_\mathrm{y}(t_\mathrm{f})$, and that we can control ϕ and ζ by means of θ and χ [see Eqs. (5)], we can now implement the SU(1, 1) Otto cycle in the superconducting circuit. To realize the two isochoric transformations, we need to couple the transmission line with the two baths, whereas the two adiabatic transformations are accomplished by tuning the Josephson energy. We observe that, with an appropriate choice of circuit parameters, we can reach a regime wherein the transmission line behaves both as Otto heat engine and as supersensitive SU(1, 1) interferometer during each adiabatic transformation. In particular, we obtain the normalized effi-

V. CONCLUSION

In this work we used mathematical tools from quantum thermodynamics and quantum metrology to investigate the performance of an SU(1, 1) quantum heat engine. This allowed us to introduce standard concepts of quantum information theory, such as the quantum Fisher information, which play a fundamental role in quantum thermodynamics (see, for example, the thermodynamic uncertainty relations [93–95]). Thus, we apply well-established protocols for phase sensitivity in the context of the performance of quantum thermal machines, an approach that has not yet been sufficiently explored.

Our quantum heat engine exploits the outstanding quantum metrological features of the SU(1, 1) interferometer in order to improve the precision in the knowledge of output observables at the cost of a reduced efficiency. Considering

that the decrease of the efficiency is inevitable in processes characterized by inner friction (in our case arising due to squeezing), the improvement of the sensitivity offers an advantage in the thermodynamic analysis of QHEs, and can also aid the design and analysis of future experimental implementations.

Finally, we applied our model to a specific superconducting transmission line, showing that it can work as a supersensitive $SU(1, 1)$ quantum heat engine. Clearly, we cannot exclude that the use of other engines in circuit QED, as well as other highly flexible quantum platforms such as Bose-Einstein condensates [96,97], may provide similar solutions with comparable or better efficiency and/or sensitivity.

[1] S. Vinjanampathy and J. Anders, Quantum thermodynamics, Contemp. Phys. **57**, 545 (2016).

[2] G. Kurizki and A. G. Kofman, *Thermodynamics and Control of Open Quantum Systems* (Cambridge University Press, Cambridge, 2022).

[3] R. Kosloff, Quantum thermodynamics: A dynamical viewpoint, Entropy **15**, 2100 (2013).

[4] F. Binder, L. A. Correa, C. Gogolin, J. Anders, and G. Adesso, *Thermodynamics in the Quantum Regime* (Springer, Cham, 2018), Vol. 195.

[5] P. P. Potts, Quantum thermodynamics, arXiv:2406.19206.

[6] S. Deffner and S. Campbell, *Quantum Thermodynamics: An Introduction to the Thermodynamics of Quantum Information* (Morgan & Claypool Publishers, San Rafael, 2019).

[7] K. Maruyama, F. Nori, and V. Vedral, Colloquium: The physics of Maxwell's demon and information, Rev. Mod. Phys. **81**, 1 (2009).

[8] H. T. Quan, Y.-X. Liu, C. P. Sun, and F. Nori, Quantum thermodynamic cycles and quantum heat engines, Phys. Rev. E **76**, 031105 (2007).

[9] H. T. Quan, Quantum thermodynamic cycles and quantum heat engines. II., Phys. Rev. E **79**, 041129 (2009).

[10] Q. Song, S. Singh, K. Zhang, W. Zhang, and P. Meystre, One qubit and one photon: The simplest polaritonic heat engine, Phys. Rev. A **94**, 063852 (2016).

[11] G. S. Agarwal and S. Chaturvedi, Quantum dynamical framework for Brownian heat engines, Phys. Rev. E **88**, 012130 (2013).

[12] D. Gelbwaser-Klimovsky, R. Alicki, and G. Kurizki, Minimal universal quantum heat machine, Phys. Rev. E **87**, 012140 (2013).

[13] D. von Lindenfels, O. Gräb, C. T. Schmiegelow, V. Kaushal, J. Schulz, M. T. Mitchison, J. Goold, F. Schmidt-Kaler, and U. G. Poschinger, Spin heat engine coupled to a harmonic-oscillator flywheel, Phys. Rev. Lett. **123**, 080602 (2019).

[14] H. Tajima and K. Funo, Superconducting-like heat current: Effective cancellation of current-dissipation trade-off by quantum coherence, Phys. Rev. Lett. **127**, 190604 (2021).

[15] S. Kamimura, H. Hakoshima, Y. Matsuzaki, K. Yoshida, and Y. Tokura, Quantum-enhanced heat engine based on superabsorption, Phys. Rev. Lett. **128**, 180602 (2022).

[16] A. U. C. Hardal, N. Aslan, C. M. Wilson, and O. E. Müstecaplıoğlu, Quantum heat engine with coupled superconducting resonators, Phys. Rev. E **96**, 062120 (2017).

[17] Q. Bouton, J. Nettersheim, S. Burgardt, D. Adam, E. Lutz, and A. Widera, A quantum heat engine driven by atomic collisions, Nat. Commun. **12**, 2063 (2021).

[18] A. Ferreri, V. Macrì, F. K. Wilhelm, F. Nori, and D. E. Bruschi, Quantum field heat engine powered by phonon-photon interactions, Phys. Rev. Res. **5**, 043274 (2023).

[19] J. Roßnagel, S. T. Dawkins, K. N. Tolazzi, O. Abah, E. Lutz, F. Schmidt-Kaler, and K. Singer, A single-atom heat engine, Science **352**, 325 (2016).

[20] D. Gelbwaser-Klimovsky and G. Kurizki, Work extraction from heat-powered quantized optomechanical setups, Sci. Rep. **5**, 7809 (2015).

[21] N. M. Myers, O. Abah, and S. Deffner, Quantum thermodynamic devices: From theoretical proposals to experimental reality, AVS Quantum Sci. **4**, 027101 (2022).

[22] K. Zhang, F. Bariani, and P. Meystre, Quantum optomechanical heat engine, Phys. Rev. Lett. **112**, 150602 (2014).

[23] K. Zhang, F. Bariani, and P. Meystre, Theory of an optomechanical quantum heat engine, Phys. Rev. A **90**, 023819 (2014).

[24] H. T. Quan, P. Zhang, and C. P. Sun, Quantum heat engine with multilevel quantum systems, Phys. Rev. E **72**, 056110 (2005).

[25] M. Youssef, G. Mahler, and A.-S. Obada, Quantum heat engine: A fully quantized model, Phys. E (Amsterdam, Neth.) **42**, 454 (2010).

[26] G. Serafini, S. Zippilli, and I. Marzoli, Optomechanical Stirling heat engine driven by feedback-controlled light, Phys. Rev. A **102**, 053502 (2020).

[27] M. Gluza, J. Sabino, N. H. Y. Ng, G. Vitagliano, M. Pezzutto, Y. Omar, I. Mazets, M. Huber, J. Schmiedmayer, and J. Eisert, Quantum field thermal machines, PRX Quantum **2**, 030310 (2021).

[28] H. Terças, S. Ribeiro, M. Pezzutto, and Y. Omar, Quantum thermal machines driven by vacuum forces, Phys. Rev. E **95**, 022135 (2017).

[29] W. Niedenzu, V. Mukherjee, A. Ghosh, A. G. Kofman, and G. Kurizki, Quantum engine efficiency bound beyond the second law of thermodynamics, Nat. Commun. **9**, 165 (2018).

[30] A. Ghosh, V. Mukherjee, W. Niedenzu, and G. Kurizki, Are quantum thermodynamic machines better than their classical counterparts?, Eur. Phys. J. Spec. Top. **227**, 2043 (2019).

[31] M. O. Scully, K. R. Chapin, K. E. Dorfman, M. B. Kim, and A. Svidzinsky, Quantum heat engine power can be increased by noise-induced coherence, Proc. Natl. Acad. Sci. USA **108**, 15097 (2011).

[32] M. O. Scully, M. S. Zubairy, G. S. Agarwal, and H. Walther, Extracting work from a single heat bath via vanishing quantum coherence, Science **299**, 862 (2003).

[33] R. Kosloff and Y. Rezek, The quantum harmonic Otto cycle, Entropy **19**, 136 (2017).

[34] S. Deffner, Efficiency of harmonic quantum Otto engines at maximal power, Entropy **20**, 875 (2018).

[35] A. Das and V. Mukherjee, Quantum-enhanced finite-time Otto cycle, Phys. Rev. Res. **2**, 033083 (2020).

[36] A. Alecce, F. Galve, N. L. Gullo, L. Dell'Anna, F. Plastina, and R. Zambrini, Quantum Otto cycle with inner friction: finite-time and disorder effects, New J. Phys. **17**, 075007 (2015).

[37] A. R. Insinga, The quantum friction and optimal finite-time performance of the quantum Otto cycle, Entropy **22**, 1060 (2020).

[38] F. Wu, J. He, Y. Ma, and J. Wang, Efficiency at maximum power of a quantum Otto cycle within finite-time or irreversible thermodynamics, Phys. Rev. E **90**, 062134 (2014).

[39] O. Abah, J. Roßnagel, G. Jacob, S. Deffner, F. Schmidt-Kaler, K. Singer, and E. Lutz, Single-ion heat engine at maximum power, Phys. Rev. Lett. **109**, 203006 (2012).

[40] J. Roßnagel, O. Abah, F. Schmidt-Kaler, K. Singer, and E. Lutz, Nanoscale heat engine beyond the Carnot limit, Phys. Rev. Lett. **112**, 030602 (2014).

[41] R. Kosloff and A. Levy, Quantum heat engines and refrigerators: Continuous devices, Annu. Rev. Phys. Chem. **65**, 365 (2014).

[42] M. Campisi and R. Fazio, The power of a critical heat engine, Nat. Commun. **7**, 11895 (2016).

[43] T. Opatrný, Bräuer, A. G. Kofman, A. Misra, N. Meher, O. Firstenberg, E. Poem, and G. Kurizki, Nonlinear coherent heat machines, Sci. Adv. **9**, eadf1070 (2023).

[44] Y. Rezek and R. Kosloff, Irreversible performance of a quantum harmonic heat engine, New J. Phys. **8**, 83 (2006).

[45] F. Plastina, A. Alecce, T. J. G. Apollaro, G. Falcone, G. Francica, F. Galve, N. Lo Gullo, and R. Zambrini, Irreversible work and inner friction in quantum thermodynamic processes, Phys. Rev. Lett. **113**, 260601 (2014).

[46] B. Yurke, S. L. McCall, and J. R. Klauder, SU(2) and SU(1,1) interferometers, Phys. Rev. A **33**, 4033 (1986).

[47] U. Seyfarth, A. B. Klimov, H. d. Guise, G. Leuchs, and L. L. Sanchez-Soto, Wigner function for SU(1,1), Quantum **4**, 317 (2020).

[48] Z. Y. Ou and X. Li, Quantum SU(1,1) interferometers: Basic principles and applications, APL Photon. **5**, 080902 (2020).

[49] M. V. Chekhova and Z. Y. Ou, Nonlinear interferometers in quantum optics, Adv. Opt. Photon. **8**, 104 (2016).

[50] A. Ferreri, M. Santandrea, M. Stefszky, K. H. Luo, H. Herrmann, C. Silberhorn, and P. R. Sharapova, Spectrally multimode integrated SU(1,1) interferometer, Quantum **5**, 461 (2021).

[51] A. Ferreri and P. R. Sharapova, Two-colour spectrally multimode integrated SU(1,1) interferometer, Symmetry **14**, 552 (2022).

[52] A. M. Marino, N. V. Corzo Trejo, and P. D. Lett, Effect of losses on the performance of an SU(1,1) interferometer, Phys. Rev. A **86**, 023844 (2012).

[53] S. Adhikari, N. Bhusal, C. You, H. Lee, and J. P. Dowling, Phase estimation in an SU(1,1) interferometer with displaced squeezed states, OSA Continuum **1**, 438 (2018).

[54] B. E. Anderson, B. L. Schmittberger, P. Gupta, K. M. Jones, and P. D. Lett, Optimal phase measurements with bright- and vacuum-seeded SU(1,1) interferometers, Phys. Rev. A **95**, 063843 (2017).

[55] W. N. Plick, J. P. Dowling, and G. S. Agarwal, Coherent-light-boosted, sub-shot noise, quantum interferometry, New J. Phys. **12**, 083014 (2010).

[56] G. Frascella, E. E. Mikhailov, N. Takanashi, R. V. Zakharov, O. V. Tikhonova, and M. V. Chekhova, Wide-field SU(1,1) interferometer, Optica **6**, 1233 (2019).

[57] D. Scharwald, T. Meier, and P. R. Sharapova, Phase sensitivity of spatially broadband high-gain SU(1, 1) interferometers, Phys. Rev. Res. **5**, 043158 (2023).

[58] C. M. Caves, Quantum-mechanical noise in an interferometer, Phys. Rev. D **23**, 1693 (1981).

[59] C. M. Caves, Quantum limits on noise in linear amplifiers, Phys. Rev. D **26**, 1817 (1982).

[60] R. Demkowicz-Dobrzański, M. Jarzyna, and J. Kołodyński, Quantum limits in optical interferometry, Prog. Opt. **60**, 345 (2015).

[61] C. Sparaciari, S. Olivares, and M. G. A. Paris, Gaussian-state interferometry with passive and active elements, Phys. Rev. A **93**, 023810 (2016).

[62] J. P. Dowling, Quantum optical metrology – the lowdown on high-N00N states, Contemp. Phys. **49**, 125 (2008).

[63] Z. Y. Ou, Fundamental quantum limit in precision phase measurement, Phys. Rev. A **55**, 2598 (1997).

[64] Y. Zheng, P. Hänggi, and D. Poletti, Occurrence of discontinuities in the performance of finite-time quantum Otto cycles, Phys. Rev. E **94**, 012137 (2016).

[65] D. E. Bruschi, A. R. Lee, and I. Fuentes, Time evolution techniques for detectors in relativistic quantum information, J. Phys. A: Math. Theor. **46**, 165303 (2013).

[66] X. Gu, A. F. Kockum, A. Miranowicz, Y. Liu, and F. Nori, Microwave photonics with superconducting quantum circuits, Phys. Rep. **718-719**, 1 (2017).

[67] D. Martínez-Tibaduiza, L. Pires, and C. Farina, Time-dependent quantum harmonic oscillator: A continuous route from adiabatic to sudden changes, J. Phys. B: At. Mol. Opt. Phys. **54**, 205401 (2021).

[68] P. Talkner, M. Campisi, and P. Hänggi, Fluctuation theorems in driven open quantum systems, J. Stat. Mech. (2009) P02025.

[69] M. Campisi, P. Talkner, and P. Hänggi, Fluctuation theorem for arbitrary open quantum systems, Phys. Rev. Lett. **102**, 210401 (2009).

[70] P. Talkner, E. Lutz, and P. Hänggi, Fluctuation theorems: Work is not an observable, Phys. Rev. E **75**, 050102(R) (2007).

[71] M. Campisi, P. Hänggi, and P. Talkner, *Colloquium*: Quantum fluctuation relations: Foundations and applications, Rev. Mod. Phys. **83**, 771 (2011).

[72] M. Manceau, G. Leuchs, F. Khalili, and M. Chekhova, Detection loss tolerant supersensitive phase measurement with an SU(1,1) interferometer, Phys. Rev. Lett. **119**, 223604 (2017).

[73] P. D. Nation, J. R. Johansson, M. P. Blencowe, and F. Nori, Colloquium: Stimulating uncertainty: Amplifying the quantum vacuum with superconducting circuits, Rev. Mod. Phys. **84**, 1 (2012).

[74] A. Blais, A. L. Grimsmo, S. M. Girvin, and A. Wallraff, Circuit quantum electrodynamics, Rev. Mod. Phys. **93**, 025005 (2021).

[75] H. T. Quan, Y. D. Wang, Y.-X. Liu, C. P. Sun, and F. Nori, Maxwell's demon assisted thermodynamic cycle in superconducting quantum circuits, Phys. Rev. Lett. **97**, 180402 (2006).

[76] J. P. Pekola, Towards quantum thermodynamics in electronic circuits, Nat. Phys. **11**, 118 (2015).

[77] B. Karimi and J. P. Pekola, Otto refrigerator based on a superconducting qubit: Classical and quantum performance, Phys. Rev. B **94**, 184503 (2016).

[78] J. Pekola and I. Khaymovich, Thermodynamics in single-electron circuits and superconducting qubits, Annu. Rev. Condens. Matter Phys. **10**, 193 (2019).

[79] A. M. Zagoskin, S. Savel'ev, F. Nori, and F. V. Kusmartsev, Squeezing as the source of inefficiency in the quantum Otto cycle, Phys. Rev. B **86**, 014501 (2012).

[80] A. M. Zagoskin, E. Il'ichev, and F. Nori, Heat cost of parametric generation of microwave squeezed states, Phys. Rev. A **85**, 063811 (2012).

[81] A. M. Zagoskin, E. Il'ichev, M. W. McCutcheon, J. F. Young, and F. Nori, Controlled generation of squeezed states of microwave radiation in a superconducting resonant circuit, Phys. Rev. Lett. **101**, 253602 (2008).

[82] A. Guthrie, C. D. Satrya, Y.-C. Chang, P. Menczel, F. Nori, and J. P. Pekola, Cooper-pair box coupled to two resonators: An architecture for a quantum refrigerator, Phys. Rev. Appl. **17**, 064022 (2022).

[83] J. R. Johansson, G. Johansson, C. M. Wilson, and F. Nori, Dynamical Casimir effect in a superconducting coplanar waveguide, Phys. Rev. Lett. **103**, 147003 (2009).

[84] J. R. Johansson, G. Johansson, C. M. Wilson, and F. Nori, Dynamical Casimir effect in superconducting microwave circuits, Phys. Rev. A **82**, 052509 (2010).

[85] C. M. Wilson, G. Johansson, A. Pourkabirian, M. Simoen, J. R. Johansson, T. Duty, F. Nori, and P. Delsing, Observation of the dynamical Casimir effect in a superconducting circuit, Nature (London) **479**, 376 (2011).

[86] N. F. Del Grosso, F. C. Lombardo, F. D. Mazzitelli, and P. I. Villar, Quantum Otto cycle in a superconducting cavity in the nonadiabatic regime, Phys. Rev. A **105**, 022202 (2022).

[87] Z. Tian, J. Jing, and A. Dragan, Analog cosmological particle generation in a superconducting circuit, Phys. Rev. D **95**, 125003 (2017).

[88] Z. Tian and J. Du, Analogue Hawking radiation and quantum soliton evaporation in a superconducting circuit, Eur. Phys. J. C **79**, 994 (2019).

[89] C. Bernard and A. Duncan, Regularization and renormalization of quantum field theory in curved space-time, Ann. Phys. (NY) **107**, 201 (1977).

[90] N. D. Birrell and P. C. W. Davies, *Quantum Fields in Curved Space* (Cambridge University Press, Cambridge, 1984).

[91] A. Ferreri, D. E. Bruschi, and F. K. Wilhelm, Particle creation in left-handed metamaterial transmission lines, Phys. Rev. Res. **6**, 033204 (2024).

[92] To avoid possible misunderstanding, we stress that the thermodynamic compression corresponds to the analog expansion of the spacetime. Vice versa, the thermodynamic expansion corresponds to the compression of the spacetime.

[93] Y. Hasegawa and T. Van Vu, Uncertainty relations in stochastic processes: An information inequality approach, Phys. Rev. E **99**, 062126 (2019).

[94] Y. Hasegawa, Quantum thermodynamic uncertainty relation for continuous measurement, Phys. Rev. Lett. **125**, 050601 (2020).

[95] Y. Hasegawa, Thermodynamic uncertainty relation for general open quantum systems, Phys. Rev. Lett. **126**, 010602 (2021).

[96] F. Dalfovo, S. Giorgini, L. P. Pitaevskii, and S. Stringari, Theory of Bose-Einstein condensation in trapped gases, Rev. Mod. Phys. **71**, 463 (1999).

[97] O. Morsch and M. Oberthaler, Dynamics of Bose-Einstein condensates in optical lattices, Rev. Mod. Phys. **78**, 179 (2006).